Nonperturbative model for optical response under intense periodic fields with application to graphene in a strong perpendicular magnetic field

J. L. Cheng[1,2] and C. Guo[1,3]

[1]*The Guo China-US Photonics Laboratory, Changchun Institute of Optics, Fine Mechanics and Physics, Chinese Academy of Sciences, 3888 Eastern South Lake Road, Changchun, Jilin 130033, China*

[2]*School of Physical Sciences, University of Chinese Academy of Sciences, Beijing 100049, China*

[3]*The Institute of Optics, University of Rochester, Rochester, New York 14627, USA*

(Received 27 December 2017; revised manuscript received 31 March 2018; published 4 May 2018)

Graphene exhibits extremely strong optical nonlinearity in a perpendicular magnetic field, the optical conductivities show complicated field dependence at a moderate light intensity, and the perturbation theory fails. The full optical currents induced by a periodic field are nonperturbatively investigated in an equation-of-motion framework based on the Floquet theorem, with the scattering described phenomenologically. The nonlinear responses are understood in terms of the dressed electronic states, or Floquet states, which could be characterized by a weak probe light field. The method is illustrated for a magnetic field at 5 T and a driving field with photon energy 0.05 eV. Our results show that the perturbation theory works for weak fields < 3 kV/cm, confirming the unusual strong light-matter interaction for Landau levels of graphene. Our approach can be easily extended to other systems.

DOI: 10.1103/PhysRevB.97.205406

I. INTRODUCTION

Landau levels (LLs) of graphene show unique properties including a large cyclotron energy $\hbar\omega_c \approx 36\sqrt{B(\text{Tesla})}$ meV and nonequidistant energies. Graphene in a strong magnetic field is suggested as a good platform for demonstrating many fundamental dynamics concepts [1], even at room temperature. Recent studies of the nonlinear responses have been extended to wavelengths in the infrared [2–7]. A huge optical susceptibility was predicted by Yao and Belyanin [3,4] and confirmed by the four-wave mixing (FWM) experiments of König-Otto *et al.* in the far infrared [5]. Proposed applications for graphene-based photonics include the generation of entangled photons [8], an all-optical switch [9], tunable lasers [6], the dynamic control of coherent pulses [10], and the demonstration of optical bistability and optical multistability [11,12].

Theoretically, optical nonlinearities are mostly studied in an equation-of-motion framework, where solutions of the dynamical equations can be obtained in the rotating wave approximation (RWA) [3,4] or by the perturbation method [7]. RWA is suitable for resonant transitions and modest incident laser intensities, which are usually discussed between the lowest several LLs. The perturbation theory can easily include the contribution from all LLs, and it works well only for weak light intensities. Both theoretical prediction [3] and experimental measurement [5] confirm that the LLs of graphene have very weak saturation fields with values around a few kV/cm. For intense light fields, the optical response could be obtained by numerical simulation, but often such calculations do not lead to physical insights into the underlying physics. In this paper, we propose to investigate the nonlinear response in the basis of Floquet states.

When electrons are driven by a periodic field at frequency Ω, nonperturbative solutions can be found for the Schrödinger equation with the inclusion of the light-matter interaction, and the electronic states are described as Floquet states from the Floquet theorem [13]. This approach is used to study the gap opening by a laser field in graphene [14–16] and Floquet topological insulators [17]. For graphene in the absence of a magnetic field, it is also employed to study the transport and linear optical properties [18–21], the dynamic Franz-Keldysh effect [19,22], and sideband effects [19]. Recently, Kibis *et al.* [23] used the Floquet theorem to study the optical and transport effects of dressed LLs of graphene by a monochromatic field. With adequate damping, the system can reach a steady state that is also periodic in time and can be probed [24] by a weak light with a different frequency ω. Generally, the response current includes components at frequencies $l\Omega$ and $l\Omega + \omega$ with integer l. Most studies focus on the response current components at frequencies Ω and ω; little attention is paid to the components at other frequencies, which are essential quantities for many nonlinear optical phenomena including third-harmonic generation (THG) and FWM.

In this paper we extend the Floquet theorem to study optical nonlinearity in the equation-of-motion framework under relaxation-time approximation, and set up a connection between the obtained expressions and the perturbation results. We apply this approach to the optical response of LLs of graphene. Due to the strong light-matter interaction, this approach is illustrated for fields below a few tens kV/cm, which can be generated by a continuous-wave laser or long duration laser pulse. For considered field strength, the relaxation-time approximation is still a widely used description [3] for scattering. As such, we discuss the nonlinear response including THG and FWM.

We organize the paper as follows. In Sec. II we derive the expressions for the response currents and conductivities from a general point of view. In Sec. III we apply the model to

graphene under a strong perpendicular magnetic field. The optical nonlinearities for its steady state are given in Sec. III A, the probe conductivities when a probe field is introduced are given in Sec. III B, and an experimental scheme for detecting and analyzing these signals is suggested in Sec. III C. In Sec. IV we conclude and discuss the possible issues to be fixed in the future.

II. METHOD

We consider the optical response of an N-level system (states labeled by Roman letters $n = 1,2,\ldots,N$) to an electric field $\boldsymbol{E}(t)$. The Hamiltonian can be written as

$$\hat{H}(t) = \hat{H}_0 + e\theta(t)\boldsymbol{E}(t)\cdot\hat{\boldsymbol{\xi}}, \tag{1}$$

where $-e$ is the electron charge, $\hat{H}_0$ is the unperturbed Hamiltonian described by a $N\times N$ matrix with elements $(\hat{H}_0)_{mn} = \varepsilon_m\delta_{mn}$, and $\hat{\boldsymbol{\xi}}$ is a matrix describing the dipole interaction. A quantity with a hat $\hat{O}$ stands for a matrix with row and column indexed by the level index n. The electric field $\boldsymbol{E}(t) = \boldsymbol{E}_{\rm drv}(t) + \boldsymbol{E}_{\rm prb}(t)$ includes a driving field $\boldsymbol{E}_{\rm drv}(t)$, which can be strong, and a probe field $\boldsymbol{E}_{\rm prb}(t)$, which is usually very weak. The light-matter interaction is turned on at $t = 0$ suddenly. The time evolution of the system is described by the equation of motion

$$\hbar\frac{\partial\hat{\rho}(t)}{\partial t} = -i[\hat{H}(t),\hat{\rho}(t)] - \hbar\gamma[\hat{\rho}(t) - \hat{\rho}^0], \tag{2}$$

where $\hat{\rho}(t)$ is a single-particle density matrix. The last term is a widely used phenomenological description of the scattering, with $\hat{\rho}^0$ the density matrix at equilibrium state and γ a relaxation parameter. We organize the formal solution as

$$\hat{\rho}(t) = \hat{\rho}^0 + \hat{\rho}_{\rm drv}(t) + \hat{\rho}_{\rm prb}(t), \tag{3}$$

$$\hat{\rho}_{\rm drv}(t) = \frac{e}{i\hbar}\int_0^t d\tau\, e^{\gamma(\tau-t)}\hat{\mathcal{U}}(t,\tau)\boldsymbol{E}_{\rm drv}(\tau)\cdot[\hat{\boldsymbol{\xi}},\hat{\rho}^0]\hat{\mathcal{U}}(\tau,t), \tag{4}$$

$$\rho_{\rm prb}(t) = \frac{e}{i\hbar}\int_0^t d\tau\, e^{\gamma(\tau-t)}\hat{\mathcal{U}}(t,\tau)\boldsymbol{E}_{\rm prb}(\tau)\cdot[\hat{\boldsymbol{\xi}},\hat{\rho}(\tau)]\hat{\mathcal{U}}(\tau,t), \tag{5}$$

where $\hat{\mathcal{U}}(t,\tau) = \sum_\alpha \psi_\alpha(t)\psi_\alpha^\dagger(\tau)$ is a unitary matrix, and $\psi_\alpha(t)$ satisfies the Schrödinger equation

$$i\hbar\partial_t\psi_\alpha(t) = [\hat{H}_0 + e\boldsymbol{E}_{\rm drv}(t)\cdot\hat{\boldsymbol{\xi}}]\psi_\alpha(t), \quad \text{for } t > 0. \tag{6}$$

Because we are only interested in the solution at $t > 0$, the factor $\theta(t)$ appearing in the Hamiltonian $H(t)$ can be ignored. Here the Greek subscript α stands for the index of the eigenstate with the inclusion of the driving field. Obviously, the unitary matrix satisfies $\hat{\mathcal{U}}(\tau,\tau) = I$. We are interested in the response current density [7] $\boldsymbol{J}(t) = -e\,{\rm Tr}[\hat{\boldsymbol{v}}\hat{\rho}(t)]$ with $\hat{\boldsymbol{v}} = [\hat{\boldsymbol{\xi}},\hat{H}(t)]/(i\hbar) = [\hat{\boldsymbol{\xi}},\hat{H}_0]/(i\hbar)$. It can be written as $\boldsymbol{J}(t) = \boldsymbol{J}_{\rm drv}(t) + \boldsymbol{J}_{\rm prb}(t)$, where $\boldsymbol{J}_{\rm drv}(t) = -e\,{\rm Tr}[\hat{\boldsymbol{v}}\hat{\rho}_{\rm drv}(t)]$ is a driving current and $\boldsymbol{J}_{\rm prb}(t) = -e\,{\rm Tr}[\hat{\boldsymbol{v}}\hat{\rho}_{\rm prb}(t)]$ is a probe current.

Here we consider a special driving field, which is periodic,

$$E^d_{\rm drv}(t) = \sum_l E^{(l);d}_{\rm drv}e^{-il\Omega t}. \tag{7}$$

The Roman superscripts stand for the Cartesian directions $\hat{\boldsymbol{x}}$ or $\hat{\boldsymbol{y}}$. Using the Floquet theorem [13], the eigenstates are Floquet states, which are dressed electronic states and can be expanded as

$$\psi_\alpha(t) = e^{-i\epsilon_\alpha t/\hbar}\sum_l e^{-il\Omega t}u^{(l)}_\alpha, \tag{8}$$

where ϵ_α is the αth quasienergy, $u^{(l)}_\alpha$ is an N-row vector, and $\{u^{(l)}_\alpha, l = \ldots,-1,0,1,\ldots\}$ forms the αth eigenvectors. They satisfy the eigenequation

$$(l\hbar\Omega + \epsilon_\alpha)u^{(l)}_\alpha = \hat{H}_0u^{(l)}_\alpha + \sum_n eE^{(n);d}_{\rm drv}\hat{\xi}^d u^{(l-n)}_\alpha. \tag{9}$$

Although $\{u^{(l+m)}_\alpha, l = \ldots,-1,0,1\ldots\}$ for integers m are also eigenstates of Eq. (9) with energies $\epsilon_\alpha + m\hbar\Omega$, they correspond to the same state $\psi_\alpha(t)$ in Eq. (6); only one of them needs to be considered. The normalization of $\psi_\alpha(t)$ gives ${\rm Tr}[\hat{\mathcal{A}}^{(l)}_{\alpha_1\alpha_2}] = \delta_{\alpha_1\alpha_2}\delta_{l,0}$ with $\hat{\mathcal{A}}^{(l)}_{\alpha_1\alpha_2} = \sum_{l_1}u^{(l_1)}_{\alpha_2}[u^{(l_1-l)}_{\alpha_1}]^\dagger$. After some algebra, we get

$$\hat{\rho}_{\rm drv}(t) = \sum_l e^{-il\Omega t}\hat{\rho}^{(l)}_{\rm drv}(t), \tag{10}$$

$$\hat{\rho}^{(l)}_{\rm drv}(t) = \sum_{\alpha_1\alpha_2 l_1}\mathcal{A}^{(l_1)}_{\alpha_2\alpha_1}G^{(l-l_1)}_{\alpha_1\alpha_2} \times[1 - e^{-\gamma t}e^{i(l-l_1)\Omega t}e^{-i(\epsilon_{\alpha_1}-\epsilon_{\alpha_2})t/\hbar}], \tag{11}$$

$$G^{(l)}_{\alpha_1\alpha_2} = \frac{e\sum_{l_2}E^{(l_2);d}_{\rm drv}{\rm Tr}\{[\hat{\xi}^d,\hat{\rho}^0]\hat{\mathcal{A}}^{(l-l_2)}_{\alpha_1\alpha_2}\}}{l\hbar\Omega - (\epsilon_{\alpha_1}-\epsilon_{\alpha_2}) + i\hbar\gamma}. \tag{12}$$

The term $\hat{\rho}^{(l)}_{\rm drv}(t)$ includes oscillating terms related to the correlations between Floquet states, but decaying with a factor $e^{-\gamma t}$. These terms correspond to damped Rabi oscillations. As $t\to\infty$, they vanish; $\hat{\rho}^{(l)}_{\rm drv}(t)$ and $\hat{\rho}_{\rm drv}(t)$ reach their steady states, which are also periodic in time. In the clean limit $\gamma\to 0$, an apparent divergence appears in the expression of $G^{(0)}_{\alpha\alpha}$, which can be shown to vanish from Eq. (9) [25]. This is not surprising because our results are the full solutions of the Schrödinger equation, which should not diverge. The asymptotic current as $t\to\infty$ is

$$J^d_{\rm drv}(t\to\infty) = \sum_l e^{-il\Omega t}J^{(l);d}_{\rm drv}, \tag{13}$$

$$J^{(l);d}_{\rm drv} = -e\sum_{\alpha_1\alpha_2 l_1}v^{(l_1);d}_{\alpha_2\alpha_1}G^{(l-l_1)}_{\alpha_1\alpha_2}. \tag{14}$$

We have used notation ${\rm Tr}[\hat{X}\hat{\mathcal{A}}^{(l)}_{\alpha_1\alpha_2}] = X^{(l)}_{\alpha_1\alpha_2}$ for $\hat{X} = \hat{v}^d$.

The effects induced by the driving field can be detected by a probe light $\boldsymbol{E}_{\rm prb}(t)$. It leads to a change of the density matrix by $\hat{\rho}_{\rm prb}(t)$, and induces a probe current density $\boldsymbol{J}_{\rm prb}(t)$. Up to the linear order of $\boldsymbol{E}_{\rm prb}$, we solve $\hat{\rho}_{\rm prb}(t)$ in Eq. (5) by setting $\hat{\rho}(\tau) = \hat{\rho}^0 + \hat{\rho}_{\rm drv}(\tau)$. The asymptotic result as $t\to\infty$ is

$$\hat{\rho}_{\rm prb}(t\to\infty) = \int\frac{d\omega}{2\pi}\sum_l e^{-il\Omega t - i\omega t}eE^b_p(\omega)\sum_{\alpha_1\alpha_2 l_1}\hat{\mathcal{A}}^{(l_1)}_{\alpha_2\alpha_1} \times\left[\mathcal{G}^{(l-l_1);b}_{\alpha_1\alpha_2}(\omega) + \mathcal{P}^{(l-l_1);b}_{\alpha_1\alpha_2}(\omega)\right], \tag{15}$$

with

$$\mathcal{G}^{(l);b}_{\alpha_1\alpha_2}(\omega)=\frac{\mathrm{Tr}\{[\hat{\xi}^b,\hat{\rho}^0]\hat{\mathcal{A}}^{(l)}_{\alpha_1\alpha_2}\}}{l\hbar\Omega+\hbar\omega-(\epsilon_{\alpha_1}-\epsilon_{\alpha_2})+i\hbar\gamma}, \quad (16)$$

$$\mathcal{P}^{(l);b}_{\alpha_1\alpha_2}(\omega)=\frac{\sum_{\alpha l_2}\left[\xi^{(l-l_2);b}_{\alpha_1\alpha}G^{(l_2)}_{\alpha\alpha_2}-G^{(l_2)}_{\alpha_1\alpha}\xi^{(l-l_2);b}_{\alpha\alpha_2}\right]}{l\hbar\Omega+\hbar\omega-(\epsilon_{\alpha_1}-\epsilon_{\alpha_2})+i\hbar\gamma}. \quad (17)$$

Here the term $\mathcal{G}$ is from $\hat{\rho}^0$, and the term $\mathcal{P}$ is from $\hat{\rho}_{\mathrm{drv}}$. The current density is then

$$J^d_{\mathrm{prb}}(t\to\infty)=\int\frac{d\omega}{2\pi}\sum_l e^{-i(l\Omega+\omega)t}\sigma^{(l);db}_{\mathrm{prb}}(\omega)E^b_{\mathrm{prb}}(\omega),$$

with the probe conductivity

$$\sigma^{(l);db}_{\mathrm{prb}}(\omega)=-e^2\sum_{\alpha_1\alpha_2 l_1}v^{(l-l_1);d}_{\alpha_2\alpha_1}\left[\mathcal{G}^{(l_1);b}_{\alpha_1\alpha_2}(\omega)+\mathcal{P}^{(l_1);b}_{\alpha_1\alpha_2}(\omega)\right]. \quad (18)$$

The quantities $J^{(l);d}_{\mathrm{drv}}$ and $J^{(l);d}_{\mathrm{prb}}(\omega)$ are experimental observable quantities, which can be extracted by measuring the light intensity of the electromagnetic radiation at frequencies $l\Omega$ and $l\Omega+\omega$, respectively. The driving field affects the probe conductivities in two aspects: One is that the quasienergies enter in the denominators of Eqs. (16) and (17). In the limit of weak relaxation, this contribution is significant around resonant peaks. The other is that the steady states of the density matrix, including both the occupations at each quasistate and the polarization between them, are changed by the driving field. The latter dominates the cases away from the resonances.

It is constructive to connect our results with the usual perturbative conductivities. Here the order l in both $J^{(l);d}_{\mathrm{drv}}$ and $\sigma^{(l);db}_{\mathrm{prb}}(\omega)$ corresponds to the response frequency $l\Omega$ and $l\Omega+\omega$, respectively, instead of the orders of the driving field. At a weak field, Eq. (9) can be solved perturbatively by treating the last term as a perturbation. In the lowest order with taking $\epsilon_\alpha\to\epsilon_n=\varepsilon_n$ and $X^{(l)}_{\alpha_1\alpha_2}\to X^{(l)}_{n_1n_2}=X_{n_1n_2}\delta_{l,0}$, $J^{(1);d}_{\mathrm{drv}}$ reduces to the perturbation results [7]. In general, the remarkable differences come from the denominator of Eqs. (12) and (17). In the limit $\gamma\to0$, the absorption edge can be changed by the driving field, which leads to the so-called dynamic Franz-Keldysh effects [22]. For a finite γ, in the regime where the perturbation theory works, this phenomenon may be smeared out. Usually, the conductivities with the contribution from $l\hbar\Omega$ may be discussed in the content of sideband effects. As we will show later, they can be associated with the nonlinear responses for weak driving fields.

III. RESULTS

We apply this approach to graphene in a strong magnetic field, $\boldsymbol{B}=B\hat{\boldsymbol{z}}$. The electronic states are LLs noted as $|\nu snk\rangle$, where $\nu=+\,(-)$ is a valley index for the $\boldsymbol{K}$ ($\boldsymbol{K}'$) valley, $s=\pm$ is a band index, $n\geqslant(1+\nu s)/2$ is a Landau index, and k is a continuum index. The eigenenergies are $E_{\nu sn}=s\varepsilon_n$, where with $\varepsilon_n=\sqrt{n}\hbar\omega_c$ with $\hbar\omega_c=\sqrt{2}\hbar v_F/l_c$ and the magnetic length $l_c=\sqrt{\hbar/(eB)}$. The energies depend on the index "sn" only. The continuum index k gives a degeneracy $\mathcal{D}=g_s/(2\pi l_c^2)$ with $g_s=2$ for spin degeneracy, and this index will be suppressed hereafter. There is no coupling between these two valleys, and the matrix elements of position and velocity operators in the νth valley can be written as $\boldsymbol{\xi}_{\nu;s_1n_1,s_2n_2}=\sum_{\tau=\pm}\xi^\tau_{\nu;s_1n_1,s_2n_2}(\hat{\boldsymbol{x}}-i\tau\hat{\boldsymbol{y}})/\sqrt{2}$ and $\boldsymbol{v}_{\nu;s_1n_1,s_2n_2}=i\hbar^{-1}(s_1\varepsilon_{n_1}-s_2\varepsilon_{n_2})\boldsymbol{\xi}_{\nu;s_1n_1,s_2n_2}$. Inversion symmetry connects the quantities in the two valleys according to $\boldsymbol{\xi}_{+;s_1n_1,s_2n_2}=s_1s_2\boldsymbol{\xi}_{-;(-s_1)n_1,(-s_2)n_2}$. Considering the Hermiticity of these quantities, all relevant matrix elements can be generated from $v^+_{+;s_1n_1,s_2n_2}=s_1v_F\delta_{n_1,n_2+1}(\delta_{n_2\neq0}/\sqrt{2}+\delta_{n_2,0}\delta_{s_2,-1})$.

In our calculations, the parameters are taken as $B=5$ T, $\hbar\Omega=0.05$ eV, the chemical potential $\mu=0$ eV, the temperature $T=10$ K, and $\hbar\gamma=10$ meV. The driving field is $\boldsymbol{E}^{(l)}_{\mathrm{drv}}=E_0\hat{\boldsymbol{x}}(\delta_{l,1}+\delta_{l,-1})$, and the density matrix at equilibrium is $\rho^0_{\nu;s_1n_1,s_2n_2}=[1+e^{(s_1\epsilon_{n_1}-\mu)/(k_BT)}]^{-1}\delta_{s_1s_2}\delta_{n_1n_2}$ with k_B the Boltzmann constant. The calculated Floquet states $\psi_\alpha(t)$ in the ν valley are denoted as $|\nu\alpha\rangle_f$ with $\alpha=-N_c,-N_c+1,\ldots,N_c-1,N_c$ and $N_c=20$ being the cutoff of the Landau index, and their quasienergies are noted as $\epsilon_{\nu\alpha}$. The driving field is taken as $E_0<60$ kV/cm, in which our results are converged for the specified N_c. The energies of the lowest several LLs are $\varepsilon_n=0$, 81, and 115 meV for $n=0$, 1, and 2, respectively. The driving photon energy does not match any of the resonant conditions.

For a linearly polarized field, the system retains the electron-hole symmetry, thus we can choose the quasienergies of the Floquet states to satisfy $\epsilon_{\nu\alpha}=-\epsilon_{\nu(-\alpha)}$, and $\epsilon_{\nu0}=0$; the occupation $[\hat{\rho}^{(l)}_{\mathrm{drv}}]_{\nu;sn,sn}$ at the LL $|\nu sn\rangle$ also satisfies $[\hat{\rho}^{(l)}_{\mathrm{drv}}]_{\nu;+n,+n}=-[\hat{\rho}^{(l)}_{\mathrm{drv}}]_{\nu;-n,-n}$ and $[\hat{\rho}^{(l)}_{\mathrm{drv}}]_{\nu;-0,-0}=0$. Furthermore, due to the crystal symmetry, the current responses $J^{(l);d}_{\mathrm{drv}}$ and $\sigma^{(l);db}_{\mathrm{prb}}(\omega)$ are nonzero only for odd order of l, and the density matrix $\rho^{(l)}_{\mathrm{drv}}(t)$ is nonzero only for even order of l. For a comparison with our previous work [7], we denote the perturbative conductivities as $\sigma^{(n)}_{\mathrm{pert}}$. In this paper, the relevant conductivities are $\sigma^{(1);xx}_{\mathrm{pert}}(\Omega)$ and $\sigma^{(3);xxxx}_{\mathrm{pert}}(\Omega,\Omega,\pm\Omega)$ for the driving field, and $\sigma^{(3);xxxx}_{\mathrm{pert}}(\Omega,\pm\Omega,\omega)$ for the probe field.

A. Current density response to the driving field

In Fig. 1 we plot the effective conductivity $\sigma^{(1)}_{\mathrm{eff}}=J^{(1);x}_{\mathrm{drv}}/E_0$ at a fundamental frequency Ω and $\sigma^{(3)}_{\mathrm{eff}}=J^{(3);x}_{\mathrm{drv}}/E_0^3$ at the third-harmonic frequency 3Ω as a function of the field amplitude E_0. We first compare these results with perturbation theory to determine the field threshold. At weak fields, up to the third order the effective conductivities are expanded as

$$\sigma^{(1)}_{\mathrm{eff}}\approx\sigma^{(1);xx}_{\mathrm{pert}}(\Omega)+3\sigma^{(3);xxxx}_{\mathrm{pert}}(\Omega,\Omega,-\Omega)E_0^2, \quad (19)$$

$$\sigma^{(3)}_{\mathrm{eff}}\approx\sigma^{(3);xxxx}_{\mathrm{pert}}(\Omega,\Omega,\Omega). \quad (20)$$

The perturbation results give $\sigma_0^{-1}\sigma^{(1);xx}_{\mathrm{pert}}=0.55-1.27i$ with $\sigma_0=e^2/(4\hbar)$, $\sigma_0^{-1}\sigma^{(3);xxxx}_{\mathrm{pert}}(\Omega,\Omega,-\Omega)=(0.128+0.0108i)\times10^{-12}$ m^2/V^2, and $\sigma_0^{-1}\sigma^{(3);xxxx}_{\mathrm{pert}}(\Omega,\Omega,\Omega)=(-1.2+0.91i)\times10^{-13}$ m^2/V^2; they are plotted in Fig. 1(a) as dashed curves. They agree with the full calculations very well when the field is $E_0<5$ kV/cm (for $\sigma^{(1)}_{\mathrm{eff}}$) or $E_0<3$ kV/cm (for $\sigma^{(3)}_{\mathrm{eff}}$) with an error less than 5%. These small thresholds indicate an extremely strong interaction between the periodic field and the LLs of graphene. For large E_0, the real part of $\sigma^{(1)}_{\mathrm{eff}}$ increases with the field with a slope slower than the perturbation results, and reaches a

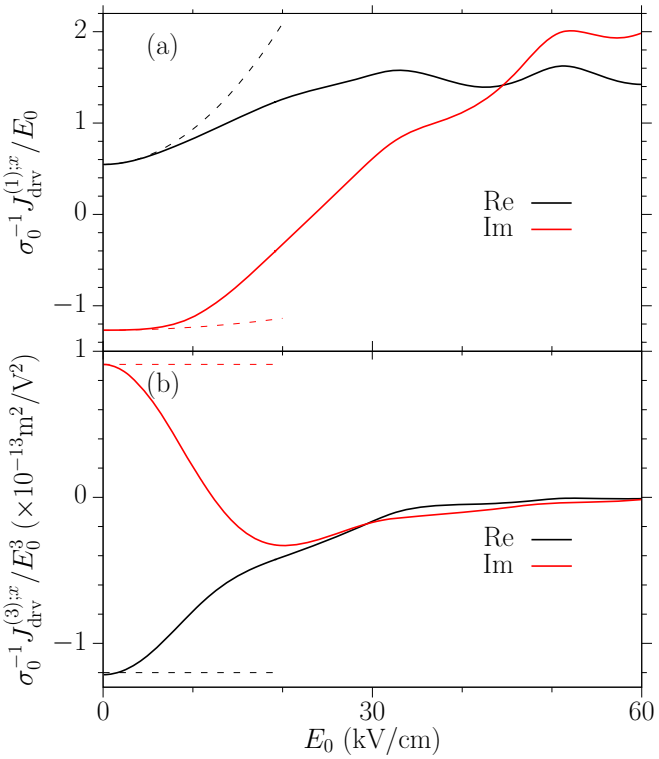

FIG. 1. Current density induced by the periodic driving field for $E_0 \leqslant 60$ kV/cm. (a) The effective linear conductivity. (b) The effective conductivity for THG. The dashed curves are perturbation results given in the right-hand side of Eqs. (19) and (20).

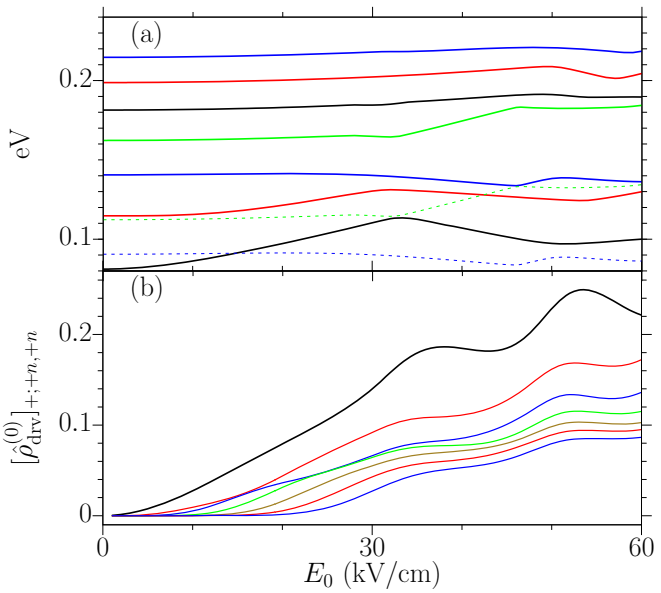

FIG. 2. (a) Field dependence of quasienergies $\epsilon_{+\alpha}$ in the $\boldsymbol{K}$ valley for $1 \leqslant \alpha \leqslant 7$. The two dashed curves correspond to the energy $\epsilon_{+\alpha} - \hbar\Omega$ for $\alpha = 3$ and 4. (b) Field dependence of the zeroth-order occupations at different LLs $|+ +n\rangle$ for $1 \leqslant n \leqslant 7$.

peak with value $1.58\sigma_0$ at $E_0 \sim 33$ kV/cm; then it shows one oscillation and arrives at another peak at $E_0 \sim 51$ kV/cm. The imaginary part of $\sigma_{\rm eff}^{(1)}$ firstly increases with the field by a larger slope, then reaches a peak around $E_0 \sim 51$ kV/cm. At $E_0 \sim 33$ kV/cm, the imaginary part shows a shoulderlike fine structure. From our discussion in Sec. II, we can understand these features from the properties of Floquet states.

In Fig. 2(a) we plot the field dependence of the quasienergies $\epsilon_{+\alpha}$ for states $|+\alpha\rangle_f$ in the $\boldsymbol{K}$ valley for $1 \leqslant \alpha \leqslant 7$. At zero field, these states correspond to the LLs $|++n\rangle$ for $1 \leqslant n \leqslant 7$. From electron-hole symmetry we can obtain their opposite energy counterparts $\epsilon_{+\alpha} = -\epsilon_{+(-\alpha)}$ and $\epsilon_{+0} = 0$. We focus on the quasistate $|+1\rangle_f$, which corresponds to the LL $|++1\rangle$ at zero field. Its quasienergy shows a complicated dependence of E_0. It starts with 81 meV at zero field, and reaches a local maximum around 113.5 meV at about $E_0 = 33$ kV/cm, then decreases to a local minimum with values 97 meV at $E_0 = 51$ kV/cm, and increases again. For small fields, the energy corrections come mostly from the LLs $|+-0\rangle$ and $|+s2\rangle$, due to the selection rules.

For strong fields, the Floquet states mix more LLs; the selection rules between Floquet states can be greatly modified from those between LLs. As an example, we analyze the behavior of the state $|+1\rangle_f$ around $E_0 \sim 33$ kV/cm. The energy of this Floquet state is close to that of $|+4\rangle_f$, which is shown in the same diagram by plotting an equivalent quasienergy $\epsilon_{+4} - \hbar\Omega$ as a dashed curve. Their interaction is allowed and leads to an anticrossing (about 1 meV splitting). Similar behavior occurs around the local minimum at $E_0 \sim 51$ kV/cm, which is induced by the interaction between the quasistates $|+1\rangle_f$ and $|+3\rangle_f$. Besides the modification of the selection rules, the strong field can also greatly change the occupations on each LL, as shown in Fig. 2(b) for the occupation $[\hat{\rho}_{\rm drv}^{(0)}(t \to \infty)]_{+;+n,+n}$ of the LL $|+sn\rangle$ for $1 \leqslant n \leqslant 7$. When $E_0 > 30$ kV/cm, the occupation at the LL $|++1\rangle$ is about 0.2, significantly deviating from its thermal equilibrium ($\sim$0). Therefore, both the quasienergies and the populations show similar tendencies as the optical conductivity $\sigma_{\rm eff}^{(1)}$, and they dominate the optical response induced by the driven field, as we discussed in Sec. II. This partly explains why the perturbation theory based on the thermal equilibrium fails.

In Fig. 1(b) we give the field dependence of the optical conductivity $\sigma_{\rm eff}^{(3)}$ for THG. Both the real and imaginary parts of $\sigma_{\rm eff}^{(3)}$ decrease quickly to very small values, and the imaginary part shows a valley around $E_0 \sim 20$ kV/cm. Similar to $\sigma_{\rm eff}^{(1)}$, $\sigma_{\rm eff}^{(3)}$ are mainly affected by the changes of optically excited populations. Its real and imaginary parts behave in a similar way because there is no specific physical process to distinguish them.

B. Probe conductivities

The effects of the intense fields on the LLs can be characterized by a weak optical field. In Fig. 3 we plot the spectra of $\sigma_{\rm prb}^{(0);xx}(\omega)$ for driving fields $E_0 = 1$, 10, 20, and 51 kV/cm. For a weak field $E_0 = 1$ kV/cm, the probe conductivities in Eq. (18) can be described perturbatively, and up to the third order it is

$$\sigma_{\rm prb}^{(0);xx}(\omega) \approx \sigma_{\rm pert}^{(1);xx}(\omega) + 6\sigma_{\rm pert}^{(3);xxxx}(\Omega, -\Omega, \omega)E_0^2. \quad (21)$$

Our calculation agrees with the perturbation results very well, indicating that the peaks in the real part can be understood by the transition between different LLs. For all three other electric

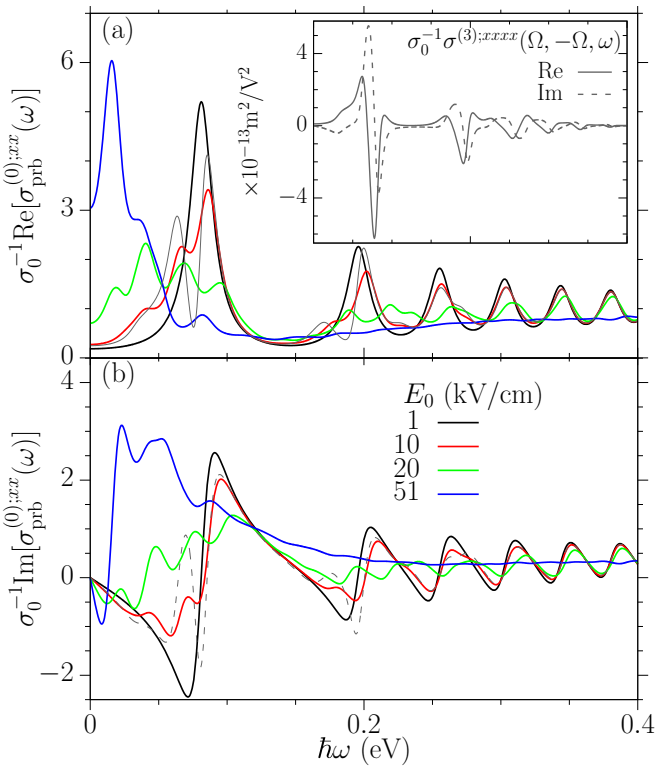

FIG. 3. The spectrum of the probe conductivity $\sigma^{(0);xx}_{\mathrm{prb}}(\omega)$ for different driving fields with (a) the real part and (b) the imaginary part. The inset in (a) shows the perturbative third-order conductivity [7] $\sigma^{(3);xxxx}(\Omega,-\Omega,\omega)$ with the x axis also in $\hbar\omega \in [0,0.4]$ eV. The gray curves in (a) and (b) are the perturbative probe conductivity up to the third order for $E_0 = 10$ kV/cm.

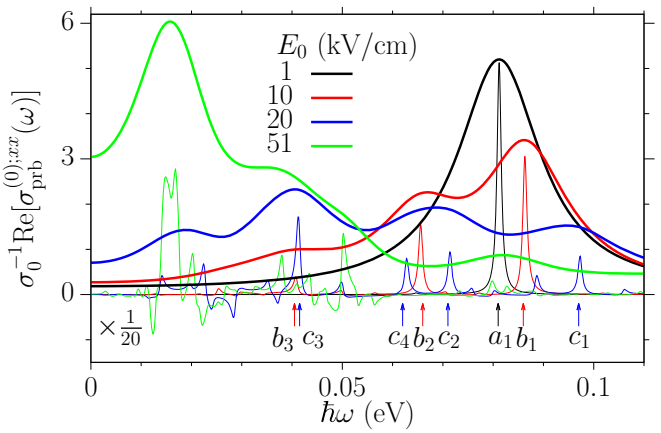

FIG. 4. The spectra of $\mathrm{Re}[\sigma^{(0);xx}_{\mathrm{prb}}(\omega)]$ for $E_0 = 1$, 10, 20, and 51 kV/cm. The relaxation parameters in Eqs. (16) and (17) are taken as 10 meV (thick curves) and 0.5 meV (thin curves, scaled by a factor 1/20), respectively. The arrows at the bottom indicate the transition peaks for the results at the smaller relaxation parameter: a_1 is for $E_0 = 1$ kV/cm, b_i is for 10 kV/cm, and c_i is for $E_0 = 20$ kV/cm.

fields, our calculations differ from the perturbation predictions significantly. As an example, the disagreement is shown for the case of $E_0 = 10$ kV/cm. This is consistent with the results in previous sections where the perturbation theory fails for fields stronger than 3 kV/cm. For $E_0 = 51$ kV/cm, most of these peaks are smeared out and a significant one appears at a very low photon energy around $\hbar\omega = 23$ meV. With increasing the driving field, the spectra manifest several features including the shift of the peak positions, the appearance of new peaks, and the lowering of the original peak values. The characterization energies, which should be related to the quasienergies of the dressed states, also become vague. This seems to contradict our analyses for Eqs. (16) and (17). They can be understood as follows: (1) The LLs of graphene are not equally spaced. At high driving field, the excited carriers enable new transition channels, which result in peaks at new photon energies. (2) With taking into account the sideband effects, the transition energies should be in a form $\epsilon_{\nu\alpha_1} - \epsilon_{\nu\alpha_2} - l\hbar\Omega$, where the integer l indicates a sideband contribution. In company with (1), the peaks become very dense, especially for intense driving fields. (3) The relaxation parameter is $\hbar\gamma = 10$ meV, which effectively broadens the transition peaks and smears out the conductivity. All these mechanisms suggest complicated energy scales involved in the system, and they are easier to be understood from the results with setting a small relaxation parameter in Eqs. (16) and (17).

Figure 4 shows the real parts of the probe conductivities with taking $\hbar\gamma = 0.5$ meV. Due to the small relaxation parameter, all peaks are sharper and narrower. The peaks at a_1, b_1, and c_1 are induced by the transitions between $|\nu 0\rangle_f \to |\nu 1\rangle_f$ and $|\nu-1\rangle_f \to |\nu 0\rangle_f$; these transitions are allowed in the absence of the driving field. Besides the position shifts due to the energy changes of the dressed states, the values of the peaks decrease too, due to the population changes. The peaks at b_2 and c_2 are induced by the sideband at $l = 1$ of the transitions between $|\nu 0\rangle_f \to |\nu 2\rangle_f$ and $|\nu-2\rangle_f \to |\nu 0\rangle_f$. Without the driving field, these transitions are forbidden due to the selection rules of LLs [7]; they become allowed because the driving field mixes the wave functions. The peaks at b_3 and c_3 are induced by the sideband at $l = 2$ of the transitions between $|\nu 0\rangle_f \to |\nu 3\rangle_f$ and $|\nu-3\rangle_f \to |\nu 0\rangle_f$; and the peak at c_4 is induced by the sideband at $m = 4$ of the transitions between $|\nu-2\rangle_f \to |\nu 3\rangle_f$ and $|\nu-3\rangle_f \to |\nu 2\rangle_f$. For the small relaxation parameter, the real parts of the probe conductivity could be negative for some photon energies, which are attributed to the energy transfer from the driving field to the probe field. With increasing the relaxation parameter to $\hbar\gamma = 10$ meV, these peaks are broadened. Two neighbor peaks merge into one if their distance is shorter than the relaxation parameter. When the electric field increases to 51 kV/cm, the wave function mixing, the sideband effects, and population changes are all greatly enhanced, and more transition peaks appear; the broadening by the relaxation parameter becomes significant. Because there are no special energy scales, these transition peaks can be thought as distributing at all photon energies randomly; for the large relaxation parameter, they are smeared out to give a smooth curve. However, due to excited populations at all dressed states, the transitions between neighbor quasilevels, which contributes like a Drude contribution, show a peak at small photon energies.

The system can also be detected by utilizing the response currents at frequencies $\omega \pm 2\Omega$, which are determined by the conductivity $\sigma^{(\pm 2);xx}_{\mathrm{prb}}(\omega)$ for FWM. The results are

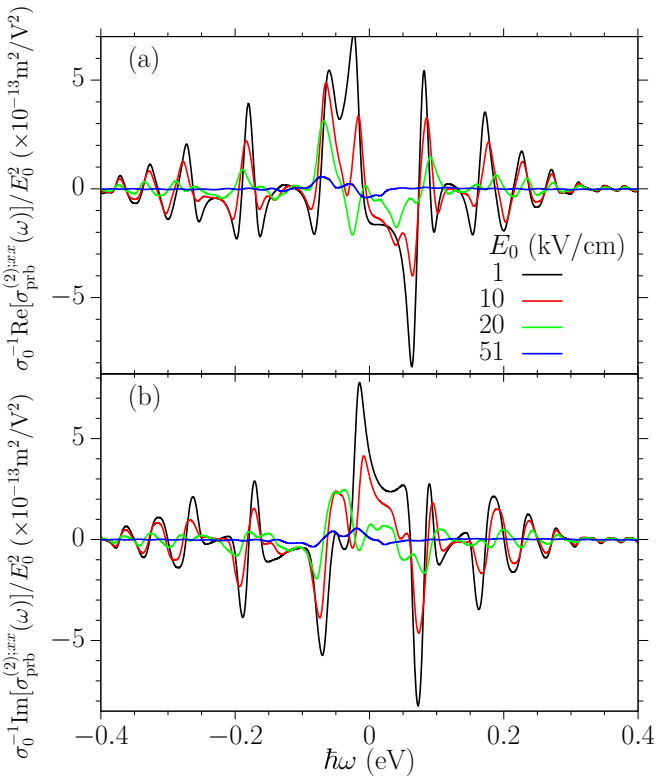

FIG. 5. The spectrum of the probe conductivity $\sigma_{\mathrm{prb}}^{(0);xx}(\omega)$ for different driving fields with (a) the real part and (b) the imaginary part.

shown in Fig. 5. At weak driving fields $E_0 = 1$ kV/cm, the results recover the perturbative conductivities $\sigma_{\mathrm{prb}}^{(2);xx}(\omega) = \sigma^{(3);xxxx}(\Omega,\Omega,\omega)$, and $\sigma_{\mathrm{prb}}^{(-2);xx}(\omega) = [\sigma^{(3);xxxx}(\Omega,\Omega,-\omega)]^*$ very well. With increasing the field strength, the spectra of this conductivity show similar behavior to those of the conductivity $\sigma_{\mathrm{prb}}^{(0);xx}(\omega)$, and they are induced by the influences of the driving field on the system.

C. A possible probe scheme

In order to connect our calculation with experiments, we propose a possible probe scheme with theoretical analyses for the radiation signal at different frequencies. A possible structure is to put a graphene sheet on top of a substrate with a refractive index $n(\omega)$. Both the driving and probe fields are normally incident from above, and the detection signals are the power of the upward radiation fields, as shown in Fig. 6.

Using the Green's function technique [26] and the transfer matrix formalism [27], the radiation field at frequency ω_1 can be expressed as

$$E(\omega_1) = E_i(\omega_1) + \frac{2}{1+n(\omega_1)} E_r(\omega_1), \tag{22}$$

$$E_r(\omega_1) = -\frac{1}{2c\epsilon_0} J(\omega_1), \tag{23}$$

where $E_i(\omega_1)$ is the incident field from above, $E(\omega_1)$ is the field experienced by the electrons in the graphene sheet, $E_r(\omega_1)$ is the field for detection, and $J(\omega_1)$ is a functional of $E(\omega)$. In our notation, $E(\Omega) = E_0$, $E(\omega) = E_{\mathrm{prb}}(\omega)$. In previous sections,

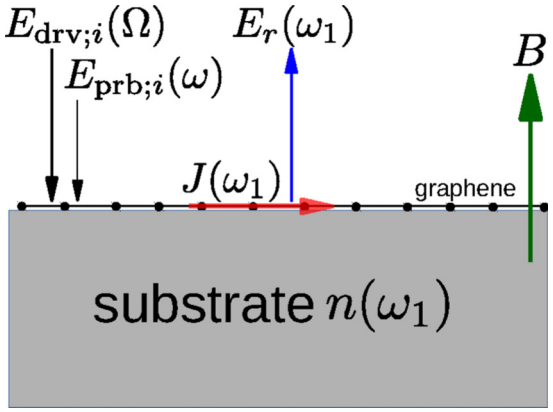

FIG. 6. Structure for detecting the radiation field. A graphene sheet is put on top of a substrate with a refractive index $n(\omega_1)$. Both the driving field $\boldsymbol{E}_{\mathrm{drv};i}(\Omega)$ and the probing field $\boldsymbol{E}_{\mathrm{prb};i}(\omega)$ are incident normally from above. The detection signal is the power of upward radiation field $E_r(\omega_1)$ generated from the response current $\boldsymbol{J}(\omega_1)$ in the graphene layer. The polarizations of both the incident fields and the detection fields are along the $\hat{\boldsymbol{x}}$ direction.

we have discussed the currents at frequencies Ω, 3Ω, ω, and $\omega \pm 2\Omega$. Here we give connections between these currents and the amplitudes of measurable fields for given incident fields.

(1) For the current $J(\Omega) = J_{\mathrm{drv}}(\Omega)$ and the radiation field $E_r(\Omega)$: The field E_0 that electrons feel in the graphene sheet is different from the incident driving field $E_{\mathrm{drv};i}(\Omega)$ due to the reaction field. From Eqs. (22) and (23) the relation between the response current and the field is

$$E_0 = E_{\mathrm{drv};i}(\Omega) - \frac{2}{1+n(\Omega)} \frac{J_{\mathrm{drv}}^{(1);x}(\Omega)}{2c\epsilon_0}. \tag{24}$$

Together with the current $J_{\mathrm{drv}}^{(1);x}(\Omega)$ induced by E_0 as shown in Fig. 1(a), both $J_{\mathrm{drv}}^{(1);x}$ and E_0 can be solved consistently. The radiation field is obtained from $E_r(\Omega) = -J_{\mathrm{drv}}^{(1);x}(\Omega)/(2c\epsilon_0)$ and further, the intensity is obtained from $I_r(\Omega) = 2c\epsilon_0|E_r(\Omega)|^2$.

(2) For the third-harmonic generation at 3Ω: There is no incident field at frequency 3Ω. With the solution E_0 obtained in the previous step, the response current at 3Ω is $J(3\Omega) = \sigma_{\mathrm{prb}}^{(0);xx}(3\Omega)E(3\Omega) + J_{\mathrm{drv}}^{(3);x}$. Setting $\omega_1 = 3\Omega$ in Eqs. (22) and (23), we get

$$E_r(3\Omega) = -\xi(3\Omega)\frac{J_{\mathrm{drv}}^{(3);x}}{2c\epsilon_0}, \tag{25}$$

where the coefficient is given by

$$\xi(\omega) = \frac{1}{1+\frac{2}{1+n(\omega)}\eta^{(0)}(\omega)} \tag{26}$$

with $\eta^{(j)}(\omega) = \sigma_{\mathrm{prb}}^{(j);xx}(\omega)/(2c\epsilon_0)$.

(3) For the reflectivity of the probe field at ω: The current is given by $J(\omega) = \sigma^{(0);xx}(\omega)E_{\mathrm{prb}}(\omega)$. Setting $\omega_1 = \omega$ in Eqs. (22) and (23), we get $E_r(\omega) = R(\omega)E_{\mathrm{prb};i}(\omega)$ with the reflectivity $R = -\eta^{(0)}(\omega)\xi(\omega)$. The total field that electrons feel in the graphene sheet is $E_{\mathrm{prb}}(\omega) = \xi(\omega)E_{\mathrm{prb};i}(\omega)$.

(4) For the FWM signal: The current for FWM is $J(\omega \pm 2\Omega) = \sigma^{(0);xx}(\omega \pm 2\Omega)E(\omega \pm 2\Omega) + \sigma^{(\pm 2);xx}(\omega)E_{\mathrm{prb}}(\omega)$;

substituting into Eqs. (22) and (23), we get

$$E_r(\omega \pm 2\Omega) = -\xi(\omega \pm 2\Omega)\eta^{(\pm 2)}(\omega)\xi(\omega)E_{\mathrm{prb};i}(\omega). \quad (27)$$

The field amplitude is determined by three conductivities $\sigma_{\mathrm{prb}}^{(0);xx}(\omega)$, $\sigma_{\mathrm{prb}}^{(0);xx}(\omega \pm 2\Omega)$, and $\sigma_{\mathrm{prb}}^{(\pm 2);xx}(\omega)$.

IV. CONCLUSION

In this study of the optical response induced by an intense periodic field, we constructed a theoretical framework based on the Floquet theorem, and derived the expressions for the full induced optical current. These expressions were used to study graphene subject to a strong perpendicular magnetic field. By comparing with a perturbation theory up to the third order, we determined the threshold field where the perturbation theory broke down. We understood these nonperturbative behaviors from the Floquet states, which could be detected by a weak light field in an optical method. We proposed an experimental scheme to observe these responses and linked the output signal with the input field and our calculated quantities. Our results can be extended to other systems.

There exist two unsolved issues in this approach: one is related to the driving field. Because most strong incident fields are laser pulses, they cannot be treated by a formalism based on fully periodic fields in a straightforward way. It would be necessary to extend the Floquet theorem to pulsed fields, even if appropriate approximations were required. The other is related to the phenomenological relaxation-time approximation used in Eq. (2). As a widely adopted approximation in perturbation theory for preliminary studies, it is not clear whether or not it can be used, or how it would be implemented for very strong fields. Although a microscopic treatment of the scattering is possible [6,28], it would still be desirable to develop simpler descriptions that might lead to more physical insight.

ACKNOWLEDGMENTS

This work has been supported by CIOMP Y63032G160, CAS QYZDB-SSW-SYS038, NSFC 61705227, and NSFC 11774340. J.L.C. acknowledges valuable discussions with Professor K. Shen and Professor J. E. Sipe.

[1] M. O. Goerbig, Rev. Mod. Phys. **83**, 1193 (2011).
[2] K. M. Rao and J. E. Sipe, Phys. Rev. B **86**, 115427 (2012).
[3] X. Yao and A. Belyanin, Phys. Rev. Lett. **108**, 255503 (2012).
[4] X. Yao and A. Belyanin, J. Phys.: Condens. Matter **25**, 054203 (2013).
[5] J. C. König-Otto, Y. Wang, A. Belyanin, C. Berger, W. A. de Heer, M. Orlita, A. Pashkin, H. Schneider, M. Helm, and S. Winnerl, Nano Lett. **17**, 2184 (2017).
[6] S. Brem, F. Wendler, and E. Malic, Phys. Rev. B **96**, 045427 (2017).
[7] J. L. Cheng and C. Guo, Phys. Rev. B **97**, 125417 (2018).
[8] M. Tokman, X. Yao, and A. Belyanin, Phys. Rev. Lett. **110**, 077404 (2013).
[9] J. Shiri and A. Malakzadeh, Laser Phys. **27**, 016201 (2017).
[10] W.-X. Yang, A.-X. Chen, X.-T. Xie, S. Liu, and S. Liu, Sci. Rep. **7**, 2513 (2017).
[11] G. Solookinejad, Phys. B **497**, 67 (2016).
[12] H. R. Hamedi and S. H. Asadpour, J. Appl. Phys. **117**, 183101 (2015).
[13] J. H. Shirley, Phys. Rev. **138**, B979 (1965).
[14] F. J. López-Rodríguez and G. G. Naumis, Phys. Rev. B **78**, 201406(R) (2008); **79**, 049901(E) (2009).
[15] H. L. Calvo, H. M. Pastawski, S. Roche, and L. E. F. F. Torres, Appl. Phys. Lett. **98**, 232103 (2011).
[16] M. Sentef, M. Claassen, A. Kemper, B. Moritz, T. Oka, J. Freericks, and T. Devereaux, Nat. Commun. **6**, 7047 (2015).
[17] J. Cayssol, B. Dóra, F. Simon, and R. Moessner, Phys. Status Solidi RRL **7**, 101 (2013).
[18] X. G. Xu, S. Sultan, C. Zhang, and J. C. Cao, Appl. Phys. Lett. **97**, 011907 (2010).
[19] Y. Zhou and M. W. Wu, Phys. Rev. B **83**, 245436 (2011).
[20] L. E. F. Foa Torres, P. M. Perez-Piskunow, C. A. Balseiro, and G. Usaj, Phys. Rev. Lett. **113**, 266801 (2014).
[21] A. Kundu, H. A. Fertig, and B. Seradjeh, Phys. Rev. Lett. **113**, 236803 (2014).
[22] A. P. Jauho and K. Johnsen, Phys. Rev. Lett. **76**, 4576 (1996).
[23] O. V. Kibis, S. Morina, K. Dini, and I. A. Shelykh, Phys. Rev. B **93**, 115420 (2016).
[24] M. Torres and A. Kunold, Phys. Rev. B **71**, 115313 (2005).
[25] Equation (9) gives $\sum_{n_1 n_2} eE_{\mathrm{drv}}^{(n_1);d}\hat{\xi}^d u_\alpha^{(n_2)}[u_\alpha^{(n_1+n_2)}]^\dagger = \sum_l (l\hbar\Omega + \epsilon_\alpha - \hat{H}_0)u_\alpha^{(l)}[u_\alpha^{(l)}]^\dagger$. By substituting this expression into the numerator of Eq. (12), it can be simplified to $[\hat{H}_0, \hat{\rho}_0]$, which is zero.
[26] J. E. Sipe, J. Opt. Soc. Am. B **4**, 481 (1987).
[27] J. L. Cheng, J. E. Sipe, N. Vermeulen, and C. Guo (unpublished).
[28] J. H. Jiang and M. W. Wu, Phys. Rev. B **75**, 035307 (2007).